

Mechanisms of Total Glucosides of Paeony in Alleviating Methotrexate-Induced Liver Injury

Guang-Yao Chen^{1,2}, Xiang-Yu Ji³, Ying Li⁴, Si-Si Zheng⁵, Qi Jin⁶, Qing-Wen Tao^{1,2}

¹Department of TCM Rheumatology, China-Japan Friendship Hospital, Beijing, 100029, People's Republic of China; ²Beijing Key Laboratory for Immune-Mediated Inflammatory Diseases, China-Japan Friendship Hospital, Beijing, 100029, People's Republic of China; ³College of Traditional Chinese Medicine, Shandong University of Traditional Chinese Medicine, Jinan, 250355, People's Republic of China; ⁴Graduate School, Beijing University of Chinese Medicine, Beijing, 100029, People's Republic of China; ⁵Beijing Key Laboratory of Mental Disorders, National Clinical Research Center for Mental Disorders & National Center for Mental Disorders, Beijing Anding Hospital, Capital Medical University, Beijing, 100088, People's Republic of China; ⁶Department of Dermatology, Beijing Hospital of Traditional Chinese Medicine, Capital Medical University, Beijing, 100010, People's Republic of China

Correspondence: Qing-Wen Tao, Department of TCM Rheumatology, China-Japan Friendship Hospital, Beijing, People's Republic of China, Tel +8613910528490, Email taoqgl@outlook.com

Objective: Total glycoside of peony (TGP) enhances methotrexate efficacy and attenuates its hepatotoxicity in rheumatoid arthritis, but the mechanisms remain unclear. This study investigates the mechanisms of TGP against methotrexate-induced liver injury through a network pharmacology-based approach.

Methods: A liver injury model was established in CD-1 mice by intraperitoneal injection of 20 mg/kg methotrexate. TGP and the positive control drug silybin were used to intervene in the methotrexate-induced liver injury model in mice. Serum ALT and AST activities, liver index test and histopathology was detected to evaluate the effects of the treatment on methotrexate-induced liver injury. Additionally, network pharmacology and serum metabolomics were employed to predict the mechanisms of TGP in treating methotrexate-induced liver injury. Experimental validation was conducted by RT-PCR, ELISA and Western blot.

Results: TGP effectively alleviated the liver index and pathological liver damage induced by methotrexate and reduced the liver injury markers, serum ALT and AST, showing effects comparable to those of the positive control drug silybin. Network pharmacology predicted that the key targets and key signaling pathways of TGP in treating methotrexate-induced liver injury are closely associated with inflammatory response. Furthermore, serum metabolomics and network pharmacology analysis indicated a close association between effects of TGP on methotrexate-induced liver injury and arachidonic acid pathway. Experimental validation results confirmed that the expression levels of IL-6, TNF and COX-2 in liver tissues were significantly elevated, with the activation of the PI3K/AKT, MAPK, and NFκB pathways. TGP intervention can reverse these changes to a certain extent.

Conclusion: TGP treatment effectively mitigates methotrexate-induced liver injury, and its mechanism is closely associated with the inhibition of hepatic inflammatory responses.

Keywords: total glucosides of paeony, methotrexate, liver injury, network pharmacology, serum metabolomics

Introduction

Drug-induced liver injury (DILI) refers to liver damage caused by drugs and their metabolites used in clinical treatment, which is one of the most common adverse drug reactions in clinical practice.¹ As a key evaluation indicator of drug safety, DILI has been paid increasing attention from researchers.² DILI includes acute liver failure, a rapid deterioration of liver function over a short period of time that can lead to eventual death.³ At the same time, in a series of chronic diseases that require long-term medication, the persistence of DILI is an important cause of liver fibrosis and liver cancer.⁴ Methotrexate (MTX) is widely used as chemotherapeutic agent and immunosuppressant in immune-related diseases and various types of cancers.^{5,6} MTX is considered irreplaceable in the management of rheumatoid arthritis (RA).⁷ However, the clinical application of MTX is often associated with a range of adverse effects, including hepatotoxicity, bone marrow suppression, gastrointestinal discomfort, nephrotoxicity, and oral mucosal ulceration.⁸ Among these, hepatotoxicity is the most common adverse reaction associated

with methotrexate therapy and is a key reason for treatment discontinuation.^{9,10} Therefore, it is essential to conduct regular monitoring of liver function during methotrexate treatment to prevent the progression to irreversible liver cirrhosis.

Paeoniae Radix Alba, the dried roots of plant *Paeonia lactiflora* Pall (Family Ranunculaceae), was a widely used traditional Chinese medicine (TCM). *Paeoniae Radix Alba* was first recorded over 2000 years ago in the TCM Classics “Shennong Bencao Jing”.¹¹ Recent pharmacological studies have demonstrated that *Paeoniae Radix Alba* exhibits significant anti-inflammatory and hepatoprotective effects.^{12–17} The total glycosides of Paeony (TGP) are active glycoside components obtained by decocting *Paeoniae Radix Alba* in water or ethanol, followed by purification using macroporous adsorption resin.^{18,19} In China, TGP Capsules (PaFuLin) have been approved by China Food and Drug Administration for the treatment of RA, and are extensively applied in clinical practice.^{20–23} High-quality clinical evidence suggests that combining TGP with methotrexate not only enhances therapeutic efficacy but also reduces clinical side effects, especially the incidence of hepatotoxicity.^{24,25} Previous studies have demonstrated that TGP effectively alleviates carbon tetrachloride (CCl₄)-induced liver injury and fibrosis in murine models.²⁶ However, to the best of our knowledge, no pharmacological studies have explored the specific mechanisms through which TGP alleviates methotrexate-induced hepatotoxicity. Therefore, this study aims to investigate the underlying mechanisms through a combination of network pharmacology and metabolomics.

Materials and Methods

Reagents and Antibodies

Phosphate buffer saline (P1012, Solarbio, China), Tissue-fixation fluid (G1101, Servicebio, China), Neutral balsam (G8590, Servicebio, China), Tris-glycine SDS-PAGE electrophoresis buffer (G2144, Servicebio, China), Tris-Glycine Transfer Buffer (G2017, Servicebio, China), Tris Buffered Saline (G0001, Servicebio, China), Tween-20 (GC204002, Servicebio, China), Nonfat dry milk (D8340, Solarbio, China), Polyvinylidene fluoride (PVDF) membranes (IPVH00010, Millipore, USA), Antibody Diluent Solution (W0003, Applygen, China), 5×Loading buffer (LT101, EpiZyme, China), Alanine aminotransferase Assay Kit (C009-2-1, Nanjing Jiancheng Institute of Bioengineering, China), Aspartate aminotransferase Assay Kit (C010-2-1, Nanjing Jiancheng Institute of Bioengineering, China), Mouse IL-6 ELISA kit (CME0006, Beijing 4A Biotech, China), Mouse TNF- α ELISA kit (CME0004, Beijing 4A Biotech, China), Mouse Total COX-2 ELISA kit (DYC4198-2, R&D Systems, USA), Hematoxylin-Eosin (HE) Stain Kit (G1120, Solarbio, China), HiPure Total RNA Mini Kit (R4011, Magen Biotechnology, China), Reverse Transcription System (A3500, Promega, USA), SYBR[®] Green Realtime PCR Master Mix (QPK-201, TOYOBO, Japan), BCA Protein Assay Kit (PC0020, Solarbio, China), PAGE Gel Fast Preparation Kit (PG112, EpiZyme, China), Chemiluminescence detection kit (SQ202, EpiZyme, China), AKT antibody (4691S, Cell Signaling, USA), p-AKT (S473) antibody (4060S, Cell Signaling, USA), NF κ B p65 (8242T, Cell Signaling, USA), p-NF κ B p65(3033S, Cell Signaling, USA), p38 MAPK antibody (A14401, Abclonal, China), p-p38 MAPK antibody (AP0526, Abclonal, China), β -Actin antibody (TA-09, Zhongshan Jingqiao Biotechnology, China), horseradish peroxidase (HRP)-conjugated goat anti-mouse IgG (ZB-5305, Zhongshan Jingqiao Biotechnology, China), HRP-conjugated goat anti-rabbit IgG (ZB-2301, Zhongshan Jingqiao Biotechnology, China). The PCR primers were purchased from Beijing Qingke Biotechnology Co., Ltd. The primer sequences are listed in Table 1.

Table 1 Polymerase Chain Reaction (PCR) Primer Sequence

Gene Name	Primer Sequence (5'to3')
Mouse TNF- α	Sense: ACAGCAAGGGACTAGCCAGGAG Antisense: AGTGCCTC TTCTGCCAGTTCCA
Mouse IL-6	Sense: CTGCAAGAGACTTCCATCCAG Antisense: AGTGGTATAGACAGGTCTGTTGG
Mouse IL-1 β	Sense: GCATCCAGCTTCAAATCTCGC Antisense: TGTTTCATCTCGGAGCCTGTAGTG
Mouse β -actin	Sense: CCTGAACCCTAAGGCCAACCG Antisense: GCTCATAGCTCTTCTCCAGGG

Model Establishment and Drug Intervention

The CD-1 mice used in this experiment were purchased from Sibeifu Biotechnology Co., Ltd. The experimental animals were housed in the animal house of China-Japan Friendship Hospital, where the feeding conditions met national standards Laboratory Animal-Requirements of Environment and Housing Facilities (GB 14925–2010, National Laboratory Animal Standardization Technical Committee of China). The experiment was approved by the Animal Ethics Committee of China-Japan Friendship Hospital (Approval No: zryhy-21-22-08-07), and all procedures involving experimental animals strictly adhered to the 3R principles (Replacement, Reduction, Refinement) to ensure ethical welfare standards.

A single intraperitoneal injection of methotrexate at a dose of 20 mg/kg was used to establish the mouse model of methotrexate-induced liver injury (MILI), as reported in previous literature.^{27–30} In this study, silybin, a commonly used plant extract for treating liver damage caused by methotrexate, was utilized as a positive control drug.³¹ The clinical dosage of TGP is typically 1.8 g/day for human adults, equivalent to 0.0257 g/kg/day based on a standard body weight of 70 kg. For silybin, the standard human dose is 0.42 g/day, corresponding to 0.006 g/kg/day. According to the body surface area conversion formula, the oral drug dose for mice calculated by body weight should be 9.1 times that of humans. Consequently, the adjusted dosages for mice were determined as 0.234 g/kg/day for TGP and 0.0546 g/kg/day for silybin. Both compounds were formulated as saline suspensions at concentrations of 23.4 mg/mL (TGP) and 5.46 mg/mL (silybin), respectively, with subsequent storage at 4°C until administration. For oral gavage administration in mice, the dosing volume was standardized at 0.1 mL per 10 g of body weight, ensuring accurate delivery of the calculated doses based on individual animal weights.

Twenty-four male CD-1 mice (6 weeks old, 35.04 ± 2.55 g body weight) were randomly allocated to four groups after 1 week of acclimatization: blank control group, methotrexate-induced liver injury group, TGP group, and silybin group. Among these, 18 mice from the methotrexate-induced liver injury group, TGP group, and silybin group underwent subsequent interventions to establish a hepatic injury model via intraperitoneal injection. The blank control group and methotrexate-induced liver injury group were gavaged with 0.1 mL of saline per 10 g of body weight at 8 AM daily. The TGP group received 0.1 mL of the prepared TGP suspension per 10 g of body weight at the same time, while the silybin group was gavaged with 0.1 mL of the prepared silybin suspension per 10 g of body weight at 8 AM daily. After 4 days of experimentation, the methotrexate-induced liver injury group, TGP group, and silybin group received an intraperitoneal injection of 20 mg/kg methotrexate solution, while the blank control group received an equivalent volume of saline. Following the experiment, whole mouse blood was collected by eyeball extirpating, and the serum was separated by centrifugation (4°C, 3000 rpm, 5 min) and stored in centrifuge tubes at –80°C. After euthanasia, the livers were excised and divided; one half was immersed in 4% paraformaldehyde for fixation for subsequent pathological analysis, while the other half was preserved at –80°C for future molecular biology experiments.

Preparation and Evaluation of Liver Histopathological Sections

The mouse liver was rinsed with pre-cooled saline and excess moisture was absorbed with filter paper. The liver was then fixed in 4% paraformaldehyde for 24 hours. Following fixation, the liver was dehydrated sequentially in 50%, 70%, 80%, and 90% ethanol, with each concentration maintained for 1 hour. The dehydrated liver was transparent by xylene solution twice (15 minutes each), followed by two immersions in paraffin solution (1 hour each). Using a microtome, the paraffin-embedded tissue was sliced into 4 µm sections, which were floated on the surface of water and placed on anti-unloading slides, baking 1 hour at 72°C. The slides were stained in hematoxylin and eosin (H&E) solution for 10 minutes and rinsed with water to remove excess stain. Finally, the slides were coverslipped with neutral resin and scanned panoramically. The histopathological scoring criteria for liver tissue are shown in Table 2.³²

Table 2 Histopathological Scoring of Liver Tissue

Score	Description
0	Normal liver tissue with no detectable lesions
1	Mild hepatocyte necrosis, slight inflammatory cell infiltration, or mild hepatocyte swelling
2	Aggregated inflammatory cell infiltration, focal hepatocyte necrosis affecting <30% of the liver lobules
3	Moderate inflammatory cell infiltration, hepatocyte necrosis affecting 30–50% of liver lobules, lobular architecture disruption
4	Extensive inflammatory cell infiltration, hepatocyte necrosis affecting >50% of liver lobules, significant lobular architecture disruption

ALT and AST Activity Assay

The serum levels of ALT and AST were detected using a colorimetric method as follows: serum samples were thawed from -80°C and melted at room temperature before being vortexed. The ALT substrate solution and AST substrate solution were incubated at 37°C for 10 minutes. In a 96-well plate, $20\ \mu\text{L}$ of the substrate solution and $5\ \mu\text{L}$ of the sample were added, mixed thoroughly, and incubated at 37°C for 20 minutes. After the reaction, $20\ \mu\text{L}$ of 2,4-dinitrophenylhydrazine solution was added to terminate the reaction, and incubated at 37°C for an additional 20 minutes. Following this, $200\ \mu\text{L}$ of $0.4\ \text{mol/L}$ sodium hydroxide solution was added, and the mixture was allowed to stand at room temperature for 15 minutes. The optical density (OD) was measured at a wavelength of $510\ \text{nm}$ using a microplate reader. The enzyme activities of ALT and AST in each sample were calculated based on the standard curve.

Network Pharmacology Prediction

The Traditional Chinese Medicine Systems Pharmacology Database and Analysis Platform (TCMSP) database (<https://old.tcmssp-e.com/>) was utilized to retrieve chemical compounds found in Paeony with “baishao” as the searching term.³³ Active compounds were identified based on the drug-likeness (DL) criterion (≥ 0.18) and oral bioavailability (OB) criterion ($\geq 30\%$).^{34–39} These compounds were then entered into the Pubchem database for their structural formulas. TCMSP database was also used to predict the potential drug targets, and the target names were standardized using the UniProt database.⁴⁰ “Methotrexate” and “liver injury” were used as the keywords for the identification of disease targets from Genecard database.⁴¹ The intersection of component targets and disease targets was defined as the key targets of TGP for the treatment of liver injury caused by methotrexate. The intersection targets obtained from the above databases were imported into Cytoscape to establish a component-disease-target network.

A protein-protein interaction (PPI) network of drug-disease intersection genes was performed using the STRING database (<https://string-db.org/Version> 12.0) to identify the most significant protein targets involved in TGP with methotrexate and liver injury.⁴² The protein with interaction score greater than 0.4 was considered statistically significant, which was then imported into Cytoscape for visualization analysis. Kyoto Encyclopedia of Genes and Genomes (KEGG) enrichment analysis was conducted using the Metascape database to pinpoint key pathways.⁴³ Pathways with $P < 0.05$ were considered to be significant and were further analyzed.

Identification of Drug Composition

The TGP were produced by Ningbo Lihua Pharmaceutical Co., LTD (Country Medicine Accurate Character Number: H20055058). The components of TGP were tested by UPLC-MS/MS for broad-spectrum plant metabolomic detection. TGP samples were freeze-dried by a freeze-dryer and ground by a grinder. $50\ \text{mg}$ sample powder was weighed using a precision electronic balance, and 70% methanol was added (pre-cooled at -20°C). After centrifuging for several vortices (4°C , $12000\times\text{g}$, 3min), the obtained supernatant was filtered using a $0.22\ \mu\text{m}$ microporous filter membrane for subsequent UPLC-MS/MS analysis.

Ultra Performance Liquid Chromatography (UPLC) (ExionLCTTM AD, <https://sciex.com.cn/>) and Tandem mass spectrometry (MS/MS) (Applied Biosystems 4500 QTRAP, <https://sciex.com.cn/>) were used for this detection. The liquid phase conditions mainly include: 1) column: Agilent SB-C18 $1.8\ \mu\text{m}$, $2.1\ \text{mm} * 100\ \text{mm}$; 2) Mobile phase: phase A is ultra-pure water (add 0.1% formic acid), phase B is acetonitrile (add 0.1% formic acid); 3) elution gradient: the proportion of B phase is 5% at $0.00\ \text{min}$, the proportion of B phase increases linearly to 95% within $9.00\ \text{min}$, and is maintained at 95% $1\ \text{min}$, $10.00\text{--}11.10\ \text{min}$, the proportion of B phase decreases to 5% , and is balanced at 5% to $14\ \text{min}$; 4) Flow rate $0.35\ \text{mL/min}$; Column temperature 40°C ; The sample size was $4\ \mu\text{L}$.

The mass spectrum conditions mainly include: electrospray ionization (ESI) temperature 550°C ; Ion spray voltage (IS) $5500\ \text{V}$ (positive ion mode) / $-4500\ \text{V}$ (negative ion mode); The ion source gas I (GSI), gas II (GSII) and gas curtain gas (CUR) are set to 50 , 60 , and $25\ \text{psi}$, respectively, and the collision-induced ionization parameters are set to high. The QQQ scan uses MRM mode and has the collision gas (nitrogen) set to medium. The mass spectrum data was processed by Analyst 1.6.3 and compared with the self-built metware database (MWDB) at Wuhan MetWare Biotechnology Co., Ltd. to identify the relevant components.

Serum Metabolomics Analysis

The metabolites from MILI group and TGP group serum samples were analyzed using an untargeted metabolomics approach, conducted by the Peking University Medical Metabolomics Platform. The obtained data were processed by removing unidentifiable metabolites and those with missing values, and then imported into the MetaboAnalyst 6.0 omics analysis website (<https://www.metaboanalyst.ca/>) for further analysis. Orthogonal partial least squares discriminant analysis (OPLS-DA) was employed to obtain inter-group differential information. Fold change (FC) values (ratios between groups) and P-values (significance of differences) were used to screen for differential metabolites. Metabolites satisfying the criteria of $|\log_2(\text{FC})| \geq 1$ and $P < 0.05$ were considered statistically significant, and the screening results were output in the form of a volcano plot. The differential metabolites that met the screening criteria were subjected to Kyoto Encyclopedia of Genes and Genomes (KEGG) enrichment analysis using the MetaboAnalyst 6.0 website. The common pathways between the metabolites' KEGG pathways and network pharmacological KEGG pathways were obtained, and a metabolite-gene target-common signaling pathway regulatory network was constructed using Cytoscape.

Quantitative Real-Time Polymerase Chain Reaction (RT-PCR)

The liver tissue was homogenized on ice using a homogenizer, and total RNA was extracted using the HiPure Total RNA Mini Kit according to the manufacturer's protocol. The RNA concentration and quality were assessed using a Nanodrop spectrophotometer. The purity of the RNA was determined by measuring the 260/280 and 260/230 absorbance ratios. The typical acceptable values for these ratios are around 1.8–2.0 for 260/280 and 2.0–2.2 for 260/230, indicating that the RNA was of sufficient quality for subsequent experiments. To prepare the RNA solution, sequentially add the following components to a microcentrifuge tube: 1 μg total RNA, 4 μL of 25 mM MgCl_2 , 2 μL of 10X Reverse Transcription Buffer, 2 μL of 10 mM dNTP Mixture, 0.5 μL of Recombinant Ribonuclease Inhibitor, 15 units of AMV Reverse Transcriptase, 0.5 μg of Oligo(dT)₁₅ Primer, and nuclease-free water to a final volume of 20 μL . Incubate the 20 μL mixture solution at 42 °C for 15 minutes to reverse transcribe into cDNA, then denature at 95 °C for 5 minutes. After cooling to 4 °C, store the cDNA at –20°C.

Mix 6.4 μL distilled water, 10 μL SYBR Green PCR Master Mix, 2 μL cDNA solution, 0.8 μL forward primer (10 μM), and 0.8 μL reverse primer (10 μM) thoroughly to prepare the reaction mixture. The PCR reaction was performed using the following conditions: an initial denaturation at 95°C for 60s, followed by 40 cycles of denaturation at 95°C for 15s, annealing at 60°C for 15s, and extension at 72°C for 45s, with data collection during the extension step. Determine the relative expression levels of each target gene using the $2^{-\Delta\Delta\text{CT}}$ method, followed by further statistical analysis.

ELISA

The liver tissue was placed in a mortar and ground into a fine powder with liquid nitrogen. An accurately weighed 50 mg of liver tissue was combined with 1 mL of PBS in a grinding tube and thoroughly homogenized on ice. After centrifugation (4°C, 3000 rpm, 5 min), 100 μL of the supernatant was carefully collected. The optical density (OD) values for each sample and standard were measured using an ELISA kit, following the manufacturer's instructions. A standard curve was generated using CurveExpert software to calculate the concentration of the target substances in each sample well.

Western Blot

RIPA lysis solution and PMSF (100 mmol/L) were mixed at a ratio of 100:1, gently shaken, and then placed on ice for storage. 100 mg of liver tissue was weighed by a precision electronic balance, which was then combined with 1 mL of the RIPA mixture and homogenized on ice using a glass homogenizer. The lysis was continued for 30 minutes on ice, followed by centrifugation (4°C, 10000 \times g, 5 minutes) to obtain the supernatant for subsequent Western blot analysis. The protein concentration of the obtained supernatant was determined using the bicinchoninic acid colorimetric (BCA) method, and the concentration was adjusted to a uniform level using RIPA mixture. The samples were mixed with a 5 \times loading buffer at a ratio of 4:1, boiled for 5 minutes at 100°C, and then centrifuged to collect the supernatant for electrophoretic analysis.

10% SDS-PAGE gel was prepared according to the manufacturer's instructions, and the electrophoresis buffer was diluted with deionized water to create a working solution. The SDS-PAGE gel was fixed in the electrophoresis tank, and the electrophoresis working solution was added. The comb was removed from the SDS-PAGE gel, and samples were

added into the wells, with pre-stained protein markers added to both sides. Electrophoresis was conducted at 150 V until the bromophenol blue indicator reached the bottom of the gel. Methanol, Tris-Glycine transfer buffer, and deionized water were mixed to prepare the transfer working solution, and the transfer working solution was pre-cooled in the refrigerator. The PVDF membrane was activated by soaking it in methanol, and a “sandwich” (sponge–filter paper–gel–membrane–filter paper–sponge) was prepared and placed in an ice bath for membrane transfer (70 V, 50 min).

TBS was added to deionized water, and Tween was included to obtain the TBST working solution. A 5% non-fat milk solution was prepared using the TBST working solution and used to block the PVDF membrane (room temperature, 1 h). The primary antibody was diluted in the antibody dilution buffer (dilution ratios are shown in Table 3) and incubated with the PVDF membrane (4°C, 12 h). After recovery of the primary antibody, the PVDF membrane was washed five times with TBST working solution and then the diluted secondary antibody (dilution ratios are detailed in Table 3) was added. Following a 1.5-hour incubation at room temperature, the membrane was washed five times with TBST working solution. The expression of the target protein was detected using a chemiluminescence imaging system. Each of the gray values of the bands was quantified using ImageJ, and the data was normalized for statistical analysis.

Data Analysis

Statistical analysis was performed using SPSS software, and graphical visualization was conducted with GraphPad Prism. Differences between groups were analyzed with the Student’s *t*-test, and $p < 0.05$ was considered statistically significant.

Results

The Effect of TGP on ALT and AST Activities in Serum of MILI Mice Model

The MILI mouse model was established by intraperitoneal injection of 20 mg/kg methotrexate, and interventions were performed with TGP and the positive control drug silybin. The results showed that the ALT and AST activities in the serum of the MILI group were significantly increased compared to those in the blank control group. After intervention with TGP and silybin, the activities of ALT and AST in serum were significantly reduced. No statistically significant difference was observed between the TGP group and the silybin group in serum ALT and AST activities (Figure 1).

The Effect of TGP on Liver Index and Liver Histopathology in MILI Mice Model

The liver index in the MILI group was significantly increased compared to the blank control group group. The liver index in the TGP group and silybin group was significantly decreased compared to the MILI group, with no statistically significant difference between the TGP group and silybin group (Figure 2A). In terms of liver pathology, liver tissue cells displayed a radial arrangement in the blank control group, with normal tissue structure and no signs of cellular degeneration or necrosis. In contrast, the MILI group showed liver damage, characterized primarily by widespread inflammatory cell infiltration, disrupted liver lobular structure, and hepatocyte swelling. After intervention with TGP and the positive control drug silybin, significant improvements were observed in inflammatory cell infiltration and the abnormalities in liver lobular structure (Figure 2B). Furthermore, the histopathological score was lower in both the TGP group and silybin group compared to the MILI group (Figure 2C).

Table 3 Antibody Dilution Ratio for Western Blotting

Antibody Name	Catalog Number	Manufacturer	Dilution Ratio
AKT antibody	4691S	Cell Signaling	1:1000
p-AKT (S473) antibody	4060S	Cell Signaling	1:1000
NF-κB p65	8242T	Cell Signaling	1:1000
p-NF-κB p65	3033S	Cell Signaling	1:1000
p38 MAPK antibody	A14401	Abclonal	1:1000
p-p38 MAPK antibody	AP0526	Abclonal	1:1000
β-Actin antibody	TA-09	Zhongshan Jingqiao Biotechnology	1:1000
HRP-conjugated goat anti-mouse IgG	ZB-5305	Zhongshan Jingqiao Biotechnology	1:5000
HRP-conjugated goat anti-rabbit IgG	ZB-2301	Zhongshan Jingqiao Biotechnology	1:5000

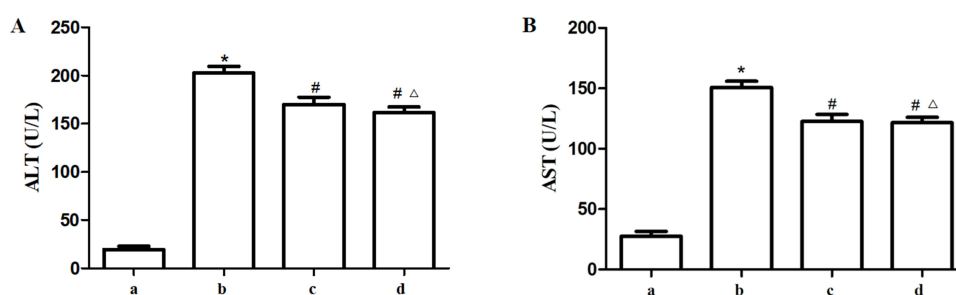


Figure 1 (A) ALT activities in the serum of mice from each group (n=6). (B) AST activities in the serum of mice from each group (n=6). a. Blank control group, b. Methotrexate-induced liver injury group, c. Total Glucosides of Paeony group, d. Silybin group. *P < 0.05 compared with the blank control group, #P < 0.05 compared with the Methotrexate-induced liver injury group, ^P > 0.05 compared with the total Glucosides of Paeony group. Experiments were repeated 6 times as a separate and independent biological replicates.

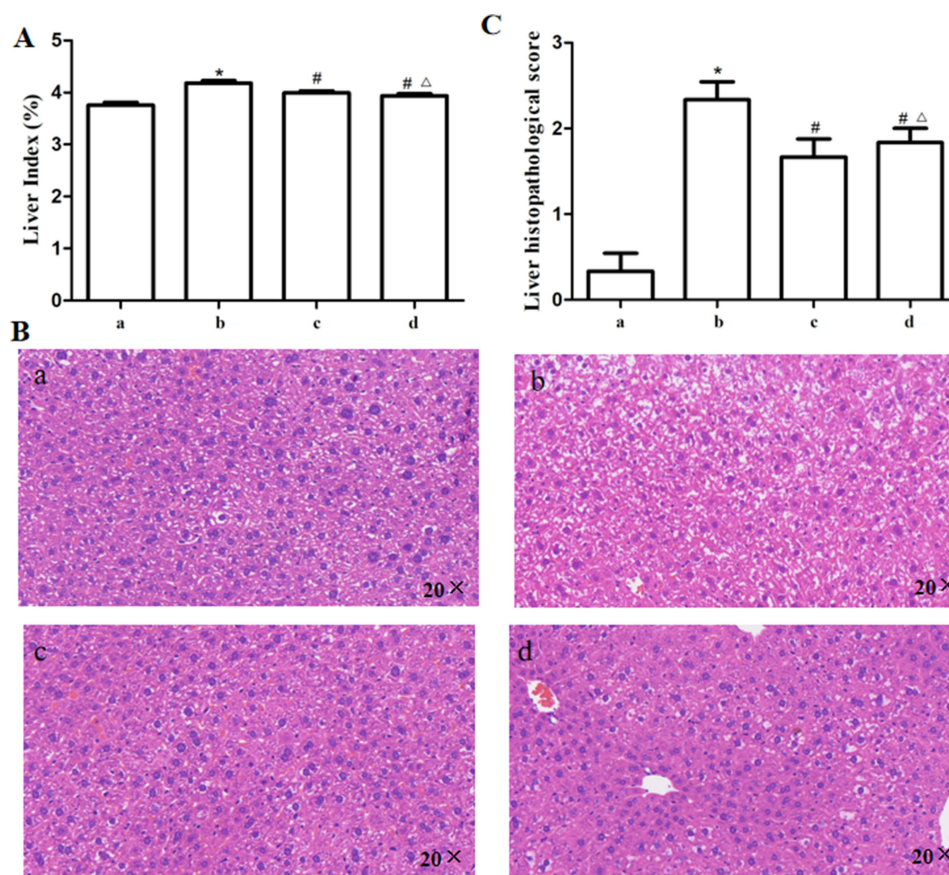


Figure 2 (A) Liver index of mice in each group (n=6). (B) Representative liver histopathological images of mice in each group. (C) Histopathological score of mice in each group (n=6). a. Blank control group, b. Methotrexate-induced liver injury group, c. Total Glucosides of Paeony group, d. Silybin group. *P < 0.05 compared with the blank control group, #P < 0.05 compared with the Methotrexate-induced liver injury group, ^P > 0.05 compared with the total Glucosides of Paeony group. Experiments were repeated 6 times as a separate and independent biological replicates.

Identification of Active Compounds from TGP

A total of 75 baishao-related targets were identified through TCMSP database. After further selection based on oral bioavailability (OB) \geq 30% and drug-likeness (DL) \geq 0.18, 13 targets were retained as active compounds, with their detailed information presented in Table 4. Using untargeted metabolomics, a total of 1558 components of TGP were identified, all 13 active components were detected in the TGP samples (Table 5 and Figure 3).

Table 4 The Basic Information on the Active Compounds of Paeoniae Radix Rubra

Name	Mol ID	Formula	MW	OB	DL
11alpha,12alpha-epoxy-3beta-23-dihydroxy-30-norolean-20-en-28,12beta-olide	MOL001910	C ₂₉ H ₄₂ O ₅	470.71	64.77	0.38
Paeoniflorgenone	MOL001918	C ₁₇ H ₁₈ O ₆	318.35	87.59	0.37
(3S,5R,8R,9R,10S,14S)-3,17-dihydroxy-4,4,8,10,14-pentamethyl-2,3,5,6,7,9-hexahydro-1H-cyclopenta[a]phenanthrene-15,16-dione	MOL001919	C ₂₂ H ₃₀ O ₄	358.52	43.56	0.53
Lactiflorin	MOL001921	C ₂₃ H ₂₆ O ₁₀	462.49	49.12	0.80
Paeoniflorin	MOL001924	C ₂₃ H ₂₈ O ₁₁	480.51	53.87	0.79
Paeoniflorin_qt	MOL001925	C ₁₇ H ₁₈ O ₆	318.35	68.18	0.40
Albiflorin_qt	MOL001928	C ₁₇ H ₁₈ O ₆	318.35	66.64	0.33
Benzoyl paeoniflorin	MOL001930	C ₃₀ H ₃₂ O ₁₂	584.62	31.27	0.75
Mairin	MOL000211	C ₃₀ H ₄₈ O ₃	456.78	55.38	0.78
Beta-sitosterol	MOL000358	C ₂₉ H ₅₀ O	414.79	36.91	0.75
Sitosterol	MOL000359	C ₂₉ H ₅₀ O	414.79	36.91	0.75
Kaempferol	MOL000422	C ₁₅ H ₁₀ O ₆	1.77	41.88	0.24
(+)-catechin	MOL000492	C ₁₅ H ₁₄ O ₆	1.92	54.83	0.24

Table 5 Detailed Information of Key Components in Total Glycosides of Paeony by LC-MS Detection

No	RT (min)	Name	Formula	Ion	Cal. m/z	Mea. m/z	Error (ppm)	MS/MS
1	4.91	Paeoniflorin_qt	C ₁₇ H ₁₈ O ₆	-	317.103	317.1038	5.788	317.1038
2	5.42	Albiflorin_qt	C ₁₇ H ₁₈ O ₆	-	317.103	317.1037	5.472	317.1037
3	6.32	Catechin	C ₁₅ H ₁₄ O ₆	-	289.0717	289.0716	3.236	289.0716, 139.0412, 123.0041
4	6.49	Lactiflorin	C ₂₃ H ₂₆ O ₁₀	-	461.1453	461.1452	2.118	461.1452
5	8.13	Kaempferol	C ₁₅ H ₁₀ O ₆	+	287.055	287.0552	2.931	287.0552, 153.0191, 121.0288
6	8.63	Paeoniflorin	C ₂₃ H ₂₈ O ₁₁	-	479.1558	479.1551	0.651	479.1551, 121.0271, 165.0539
7	10.08	Paeoniflorgenone	C ₁₇ H ₁₈ O ₆	-	317.103	317.1039	6.103	317.1039
8	10.33	Benzoyl paeoniflorin	C ₃₀ H ₃₂ O ₁₂	-	583.182	583.1822	2.053	583.1822
9	12.26	(3S,5R,8R,9R,10S,14S)-3,17-dihydroxy-4,4,8,10,14-pentamethyl-2,3,5,6,7,9-hexahydro-1H-cyclopenta[a]phenanthrene-15,16-dione	C ₂₂ H ₃₀ O ₄	-	357.2071	357.2076	4.379	357.2076, 329.2133, 301.2201
10	16.13	11alpha,12alpha-epoxy-3beta-23-dihydroxy-30-norolean-20-en-28,12beta-olide	C ₂₉ H ₄₂ O ₅	-	469.2959	469.2951	0.531	469.2951
11	16.26	Mairin	C ₃₀ H ₄₈ O ₃	+	455.353	455.3533	2.917	455.3533, 315.1791, 203.1766
12	20.72	Sitosterol	C ₂₉ H ₅₀ O	+	415.3934	415.3931	-0.825	415.39311, 119.0851, 79.0213
13	20.91	Beta-sitosterol	C ₂₉ H ₅₀ O	+	415.3934	415.3932	-0.584	415.3932, 119.0852, 79.0213

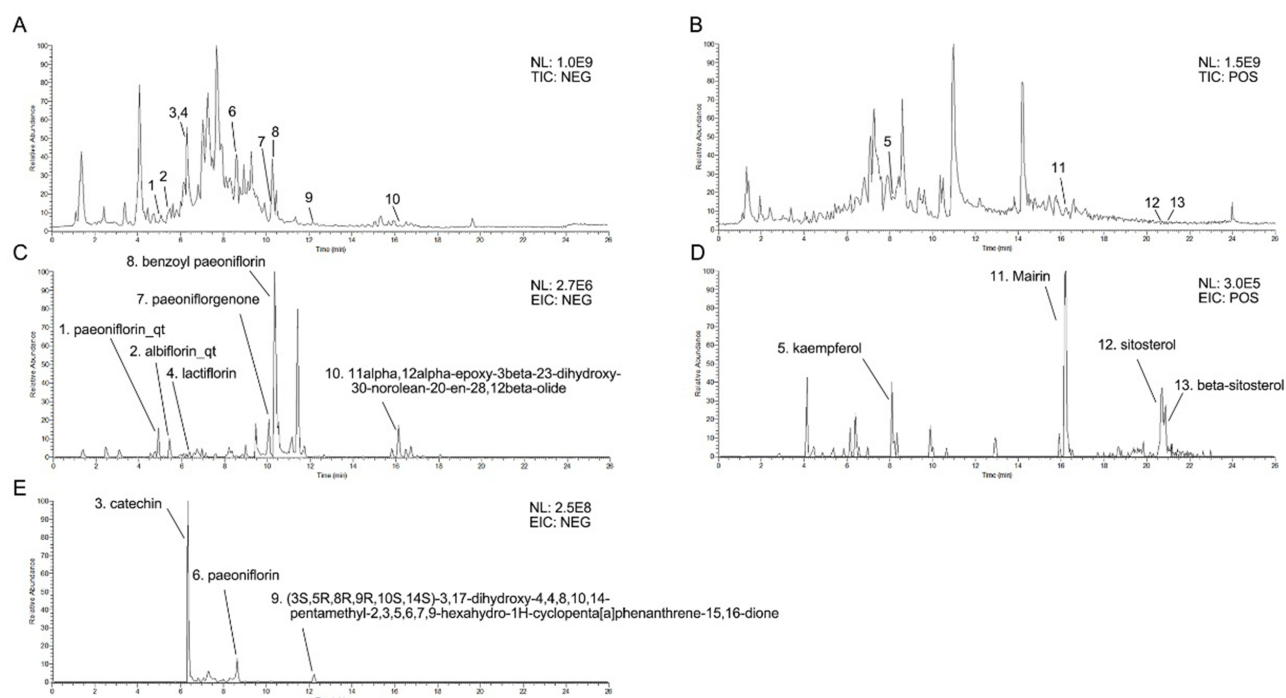


Figure 3 Identification of active compounds of total Glucosides of Paeyon with LC-MS. (A) Total ion chromatography on negative; (B) Total ion chromatography on positive; (C) Identification of paeoniflorin_qt, albfiflorin_qt, Lactiflorin, paeoniflogenon, benzoyl paeoniflorin, 11alpha, 12alpha-epoxy-3beta-23-dihydroxy-30-norolean-20-en-28, 12beta-olide; (D) kaempferol, Mairin, sitosterol, beta-sitosterol; (E) catechin, paeoniflorin, (3S,5R,8R,9R,10S,14S)-3,17-dihydroxy-4,4,8,10,14-pentamethyl-2,3,5,6,7,9-hexahydro-1H-cyclopenta[a]phenanthrene-15,16-dione.

The CT-Network for TGP Treatment of Methotrexate-Induced Liver Injury

A total of 134 targets for 13 active compounds from the TCMSP database were identified. Additionally, 3359 methotrexate-related targets and 1735 liver injury-related targets were retrieved from the Genecards database (Figure 4A). The intersection targets associated with TGP active compounds, methotrexate or liver injury were defined

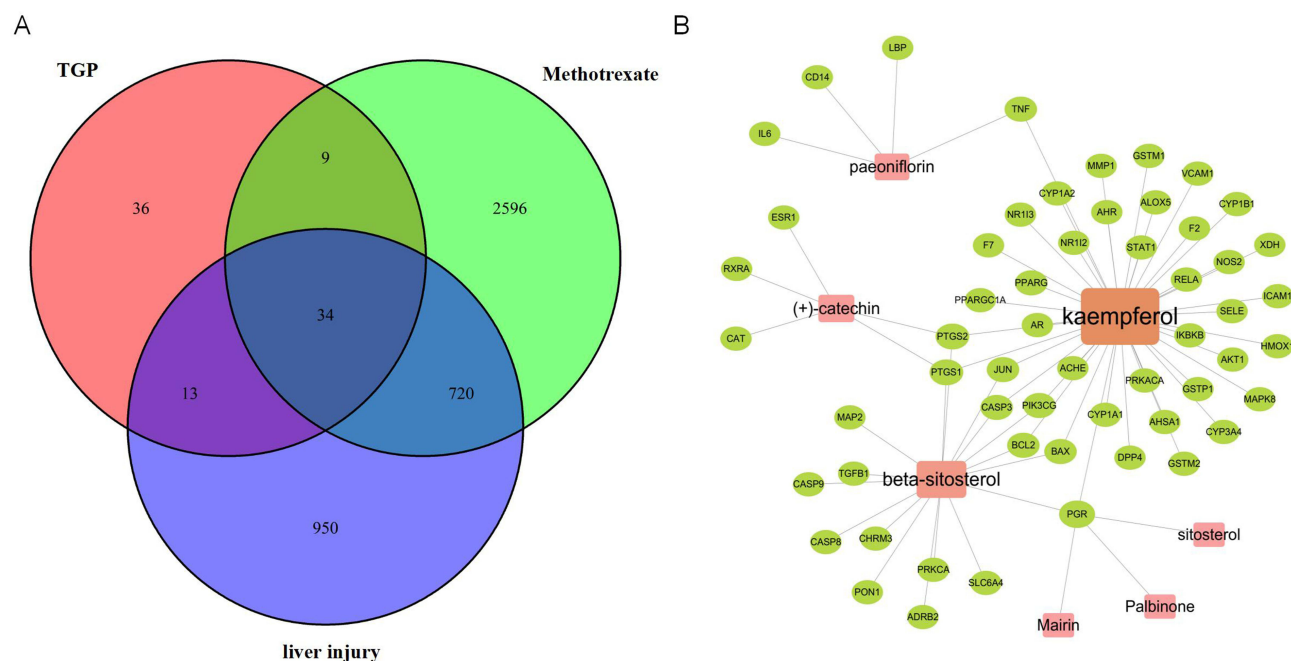


Figure 4 (A) Venn diagram of the number of targets for total Glucosides of Paeyon, methotrexate, and liver injury. (B) Compound-target network of total Glucosides of Paeyon in the treatment of methotrexate-induced liver injury.

as the therapeutic targets for TGP treatment of methotrexate-induced liver injury. A CT-network for TGP treatment of methotrexate-induced liver injury was constructed by Cytoscape 3.10.3, which contained 56 therapeutic targets, 7 related TGP active compounds and 70 edges. Results showed that PGR had the highest number of connections with targets, followed by PTGS1 and PTGS2, suggesting that those were the potential key targets of TGP against methotrexate-induced liver injury (Figure 4B).

Key Targets of TGP in the Treatment of Methotrexate-Induced Liver Injury

A PPI analysis was conducted on the targets for TGP treatment of methotrexate-induced liver injury. In this PPI network, there were 50 nodes connected by 207 edges. The PPI results were visualized using Cytoscape (Figure 5A). The top 10 targets ranked by the number of connections include IL6, AKT1, TNF, JUN, PTSG2, BCL2, RELA, CASP3, ESR1 and PPARG (Figure 5B).

Key Pathway of TGP in the Treatment of Methotrexate-Induced Liver Injury Through KEGG Enrichment Analysis

KEGG enrichment analysis was performed on the targets for TGP treatment of methotrexate-induced liver injury, and a total of 158 related signal pathways with $P < 0.05$ were obtained. After removing disease-related and metabolism-related pathways, the top 12 signaling pathways include the TNF signaling pathway, Toll-like receptor signaling pathway, TNF signaling pathway, Apoptosis, MAPK signaling pathway, IL-17 signaling pathway, C-type lectin receptor signaling pathway, NF κ B signaling pathway, Th17 cell differentiation, Relaxin signaling pathway, Osteoclast differentiation, NOD-like receptor signaling pathway, PI3K-Akt signaling pathway (Figure 6A). The associations between these 12 signaling pathways and related targets were constructed using Cytoscape. The genes with the highest frequency of occurrence include RELA, IKBKB, MAPK8, JUN, TNF, AKT1, IL6, CASP8, STAT1, BCL2, TAFB1 and PTGS2 (Figure 6B).

Screening of Differential Metabolites in Serum

The serum metabolomic results from the MILI group and the TGP group were analyzed. The OPLS-DA plots for the two groups are shown in Figure 7A. A total of 267 differential metabolites with $P < 0.05$ and $FC \geq 2$ or $FC \leq 0.5$ were screened out from the two groups, among which 51 metabolites were upregulated and 221 were downregulated in the TGP group. The volcano plot depicting these differential metabolites is presented in Figure 7B. The hierarchical clustering heatmap of the top 50 differential metabolites is shown in Figure 7C.

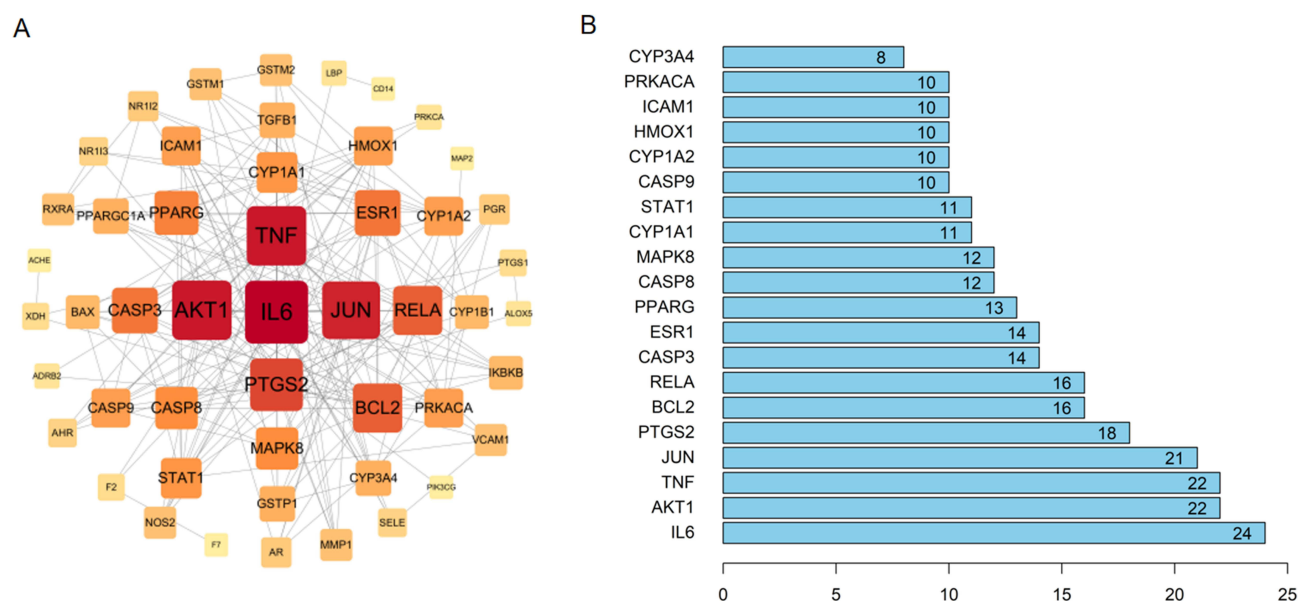


Figure 5 (A) Visualization of the protein-protein interaction network using Cytoscape. (B) Top 20 targets related to total Glucosides of Peony treatment of methotrexate-induced liver injury.

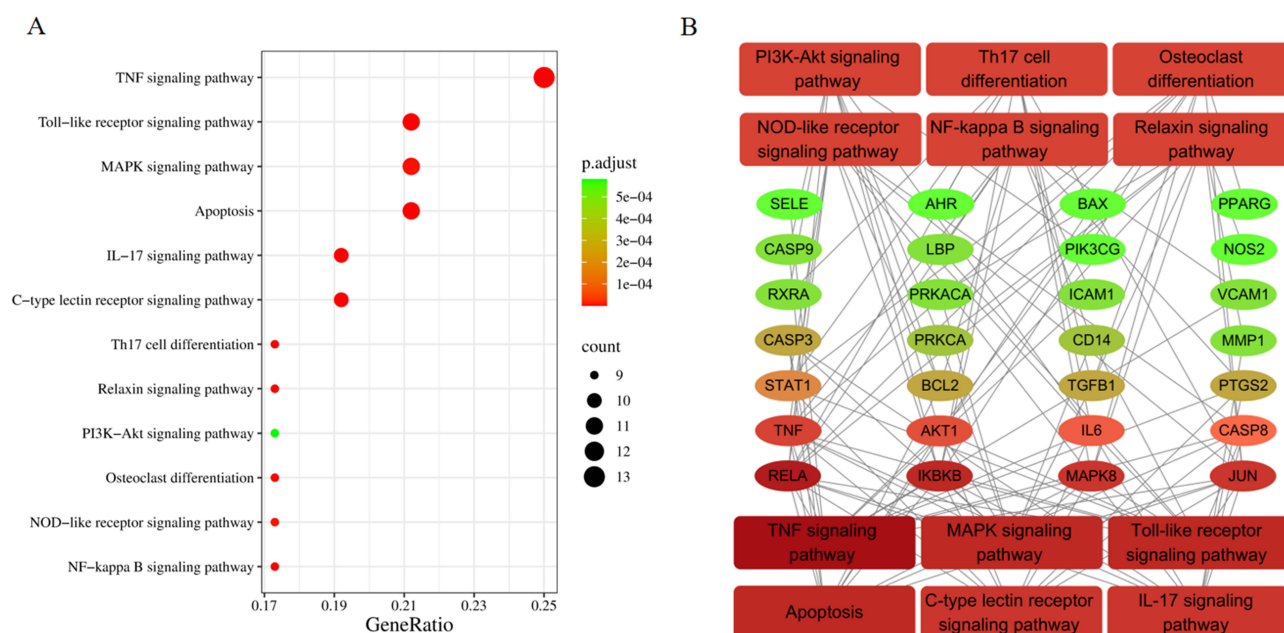


Figure 6 (A) Top 15 Signaling Pathways of KEGG Enrichment Analysis. **(B)** Relationship Between Signaling Pathways and Targets.

KEGG Enrichment Analysis of Metabolomics

The differential metabolites obtained from metabolomics were subjected to KEGG analysis, resulting in the enrichment of 38 metabolism-related pathways (Figure 8A). By intersecting these pathways with those related to the targets of TGP treatment of methotrexate-induced liver injury, four common signaling pathways were identified, including Tryptophan metabolism, Glutathione metabolism, Arachidonic acid metabolism, and Steroid hormone biosynthesis (Figure 8B). The associations between these common signaling pathways, metabolites, and genes are shown in Figure 8C.

Expression of TNF- α , IL-6, and COX-2 mRNA and Protein in Liver Tissue

The expression of TNF- α , IL-6 and COX-2 mRNA in the liver of mice from each group was detected by RT-PCR and ELISA. The results showed that the mRNA levels of TNF- α , IL-6, and COX-2 in the liver of the MILI group were significantly increased compared to the blank control group. After treatment with TGP and silybin, the mRNA levels of TNF- α , IL-6, and COX-2 in the liver were significantly reduced (Figure 9).

Western Blot Analysis

Western Blot results showed that there were no significant changes in the expression of NF κ B p65, p38 MAPK and AKT among the groups. In the MILI group, the levels of p-NF κ B p65, p-AKT and p-p38 MAPK were significantly increased compared to the blank control group, suggesting that PI3K/AKT, NF κ B and MAPK signaling pathways were abnormally activated in the liver tissue after methotrexate intervention. Treatment with TGP or Silybin was able to partially inhibit the activation of the PI3K/AKT, NF κ B and MAPK signaling pathways (Figure 10).

Discussion

By competitively inhibiting the activity of dihydrofolate reductase, methotrexate blocks the conversion of folate to tetrahydrofolate, thus interfering with the synthesis of nucleic acids, resulting in DNA damage and cell apoptosis.⁴⁴ Therefore, methotrexate has a direct effect on inhibiting the activity of tumor cell proliferation.^{45,46} Based on the same biological mechanism, methotrexate exerts an inhibitory effect on immune-related cells including lymphocytes and monocytes-macrophages, leading to immunosuppressive effects.^{47,48} Although the pharmacological mechanism of methotrexate in inducing hepatotoxicity has not been fully elucidated, existing studies suggest a close association with direct hepatocyte damage.⁴⁹ After initiating methotrexate therapy, the patient's liver function must be monitored

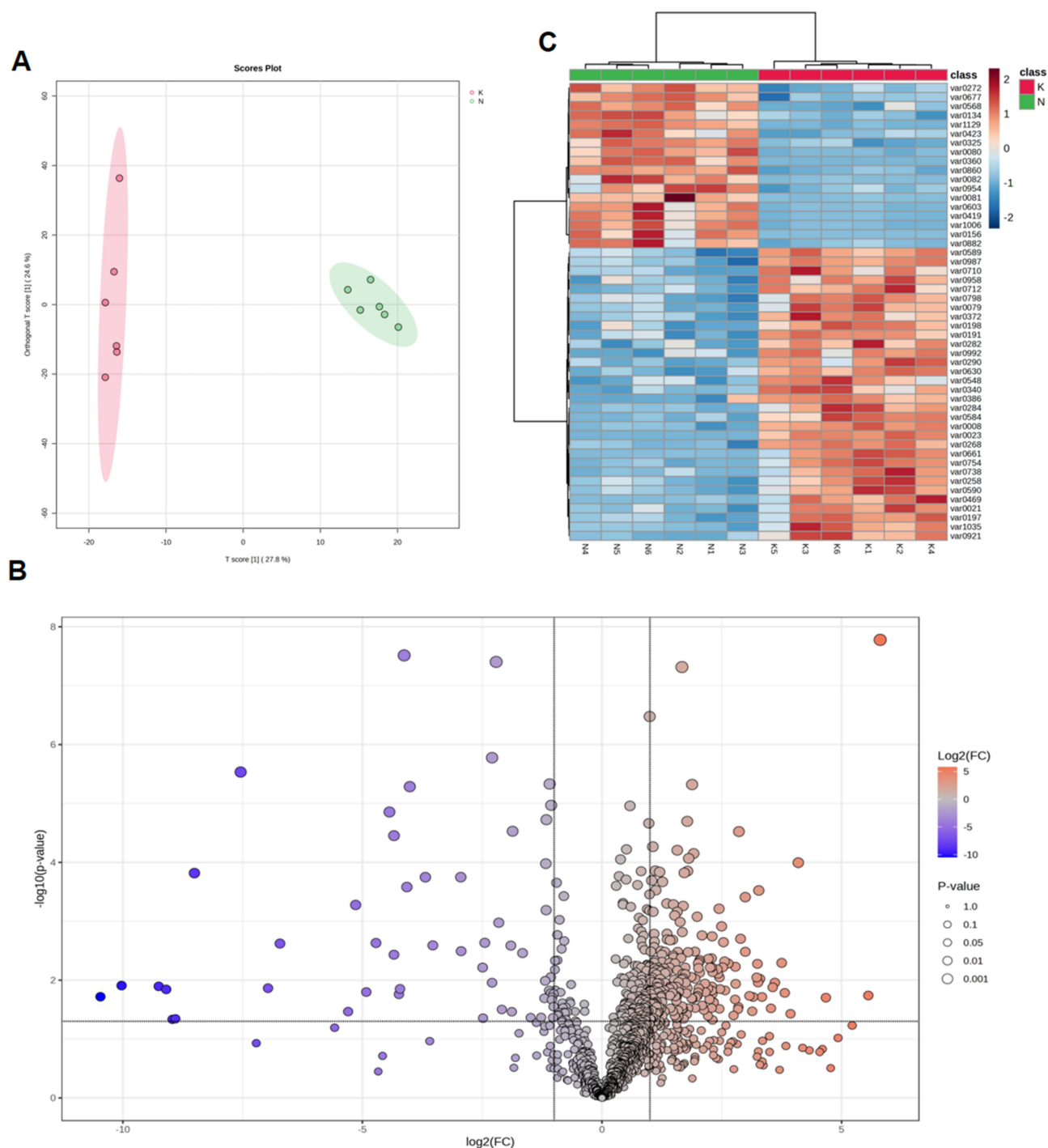


Figure 7 Differential analysis of serum metabolomics between Methotrexate-induced liver injury group and total Glucosides of Peony group (n=6). **(A)** OPLS-DA plot for the two groups. **(B)** Volcano plot of differential metabolites. **(C)** Hierarchical clustering heatmap of the top 50 differential metabolites.

regularly.⁵⁰ For patients with mild methotrexate-induced liver function impairment, a combination of hepatoprotective drugs can be used, while severe cases may require discontinuation of treatment.

As a Disease-Modifying Anti-Rheumatic Drugs (DMARDs) for RA, TGP can reduce the disease activity in RA patients. The combined use of TGP and methotrexate in the treatment of RA can achieve synergistic effects and reduce toxicity. Further exploration of the pharmacological mechanism of TGP in alleviating methotrexate-induced hepatotoxicity is helpful for its clinical application. Hepatocyte apoptosis is a hallmark of liver injury, which results in the release of

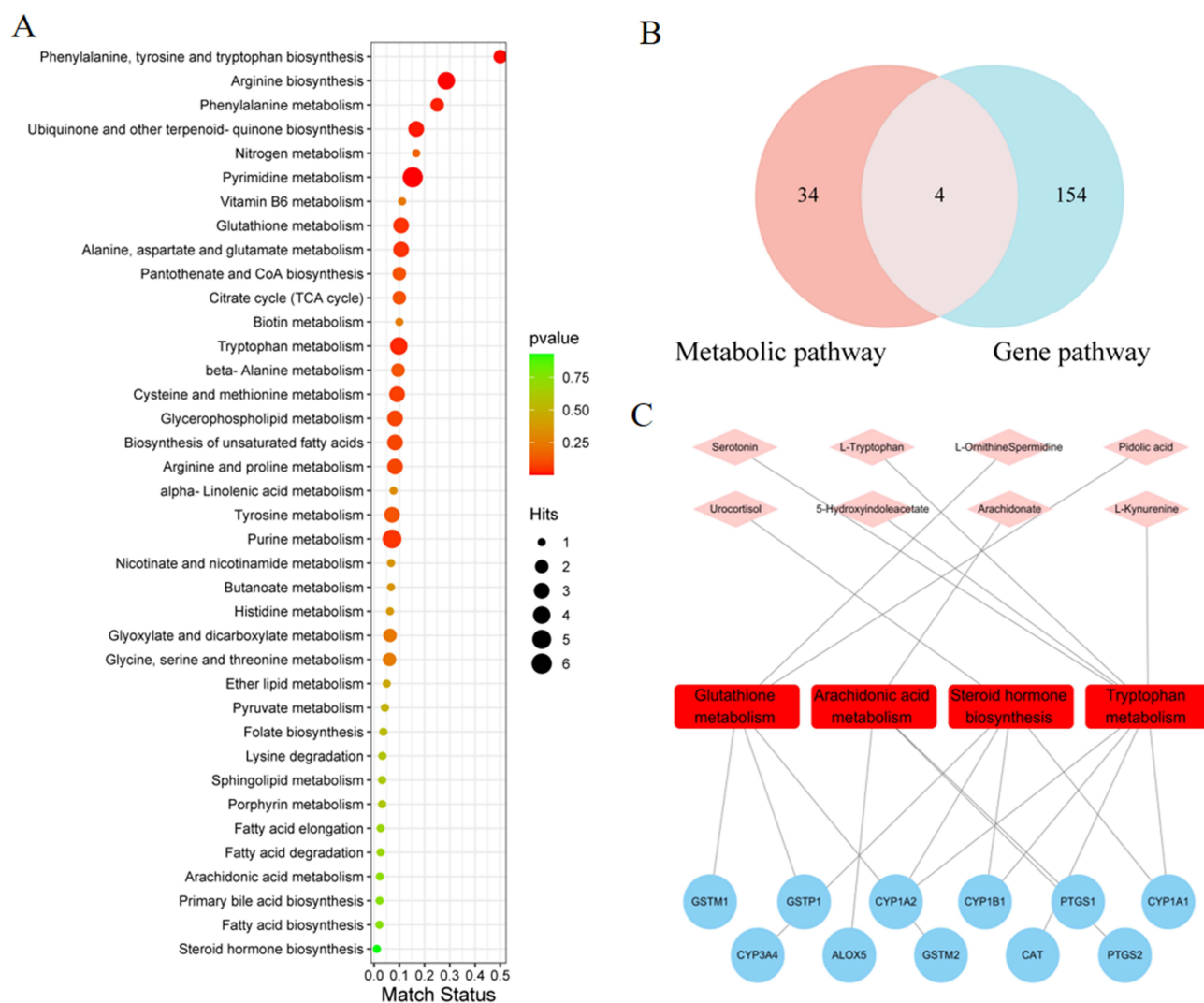


Figure 8 (A) KEGG enrichment analysis of differential metabolites. (B) Venn diagram illustrating the common pathways between the KEGG enrichment analysis of metabolomics and the KEGG enrichment analysis related to TGP treatment of methotrexate-induced liver injury targets. (C) Associations between common signaling pathways, metabolites, and genes.

mitochondrial enzymes such as ALT (Alanine aminotransferase) and AST (Aspartate transaminase) into the serum, which were used to evaluate liver functions. In this study, we confirmed through animal experiments that TGP can effectively reduce the expression of serum aminotransferase caused by methotrexate. Liver pathology further confirmed that methotrexate-induced liver damage is characterized by extensive hepatocyte apoptosis and inflammatory cell infiltration. These pathological changes can be reversed by TGP intervention.

Network pharmacology is a comprehensive approach based on systems biology analysis, providing a holistic method to uncover the complex mechanisms of multi-component drugs, diseases, and signaling pathways. In the subsequent study, we identified the key components of TGP and conducted a network pharmacology analysis. The analysis indicated that the key targets of TGP in the treatment of methotrexate-induced liver injury were closely associated with inflammatory factors such as IL-6, TNF, and COX-2. Additionally, key proteins involved in inflammatory signaling pathways, including AKT1, RELA, CASP3, MAPK8, STAT1, and CASP9, were also identified. Furthermore, KEGG enrichment analysis revealed that TGP's therapeutic effects on methotrexate-induced liver injury involve cellular apoptosis and several inflammatory signaling pathways, including the TNF signaling pathway, Toll-like receptor signaling pathway, IL-17 signaling pathway, NF- κ B signaling pathway, Th17 cell differentiation, MAPK signaling pathway, NOD-like receptor signaling pathway, and HIF-1 signaling pathway. The integration of network pharmacology and serum metabolomics suggested that Arachidonic acid

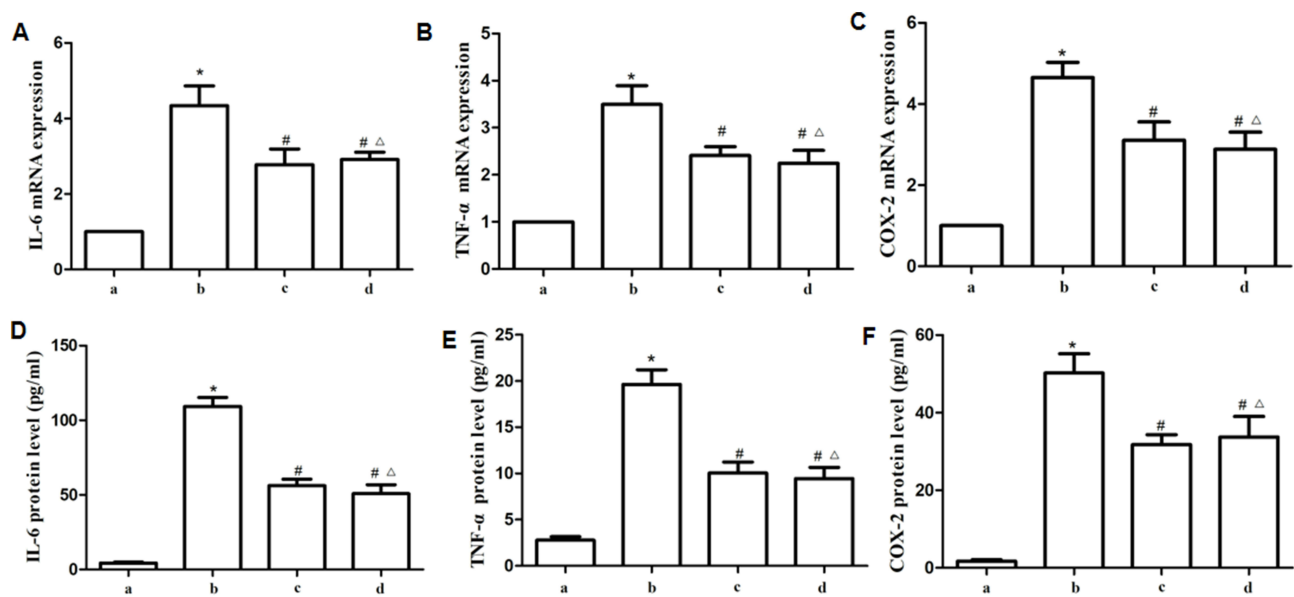


Figure 9 (A and D) Expression of IL-6 mRNA and protein in the liver of mice from each group (n=6). (B and E) Expression of TNF- α mRNA and protein in the liver of mice from each group (n=6). (C and F) Expression of COX-2 mRNA and protein in the liver of mice from each group (n=6). a. Blank control group, b. Methotrexate-induced liver injury group, c. Total Glucosides of Paeony group, d. Silybin group. *P < 0.05 compared with the blank control group, #P < 0.05 compared with the Methotrexate-induced liver injury group, Δ P > 0.05 compared with the total Glucosides of Paeony group. Experiments were repeated 6 times as a separate and independent biological replicates.

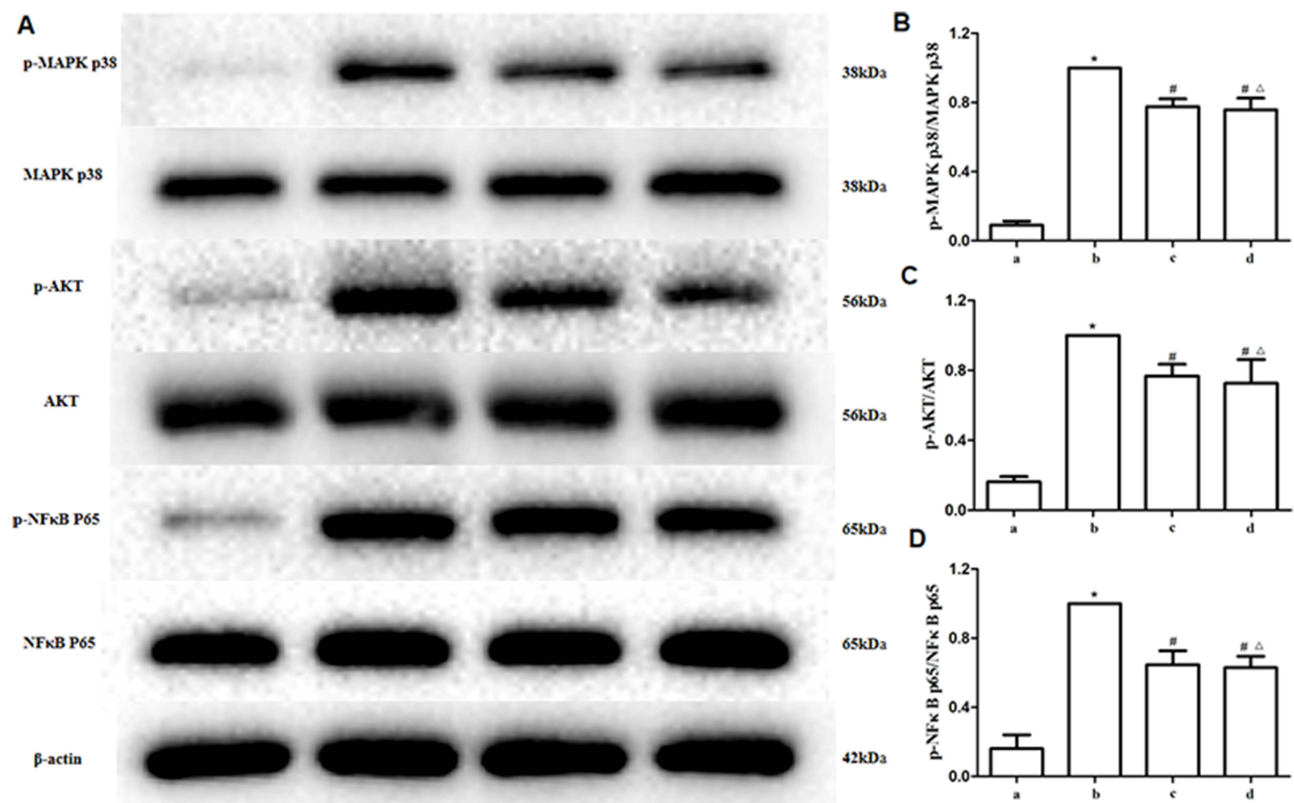


Figure 10 (A) Representative Western blot images. (B) Statistical analysis of p-MAPK p38/MAPK p38 in each group (n=6). (C) Statistical analysis of p-AKT/AKT in each group (n=6). (D) Statistical analysis of p-NF κ B p65/NF κ B p65 expression in each group (n=6). a. Blank control group, b. Methotrexate-induced liver injury group, c. Total Glucosides of Paeony group, d. Silybin group. *P < 0.05 compared with the blank control group, #P < 0.05 compared with the Methotrexate-induced liver injury group, Δ P > 0.05 compared with the total Glucosides of Paeony group. Experiments were repeated 6 times as a separate and independent biological replicates.

metabolism and Steroid hormone biosynthesis, both related to inflammatory responses, play key roles in the therapeutic effects of TGP on methotrexate-induced liver injury. There exists a close interplay between hepatic injury and inflammatory responses. Hepatocyte damage can trigger an immune system-mediated inflammatory cascade, while the sustained inflammatory microenvironment further exacerbates hepatic pathological progression through oxidative stress and cytokine storm.^{51,52} Through a comprehensive review of previous literature, we have identified that TGP exerts anti-inflammatory effects in other experimental models by suppressing the aforementioned signaling pathways, thereby elucidating its molecular mechanisms underlying inflammatory response inhibition.^{53–56}

Based on the predictions from network pharmacology and serum metabolomics, along with a review of the existing literature, we propose the following mechanism for TGP in the treatment of methotrexate-induced liver injury. The cytotoxic effects of methotrexate activate the necrotic process in hepatocytes, releasing large amounts of cellular contents and inducing an excessive inflammatory response in liver tissue. The inflammatory response in liver cells leads to the release of numerous inflammatory factors, activation of inflammation-related signaling pathways, and infiltration of inflammatory cells into the liver, further accelerating hepatocyte necrosis. Among the predicted pathways and targets, the PI3K/AKT signaling pathway, Toll-like receptor signaling pathway, MAPK signaling pathway, and NOD-like receptor signaling pathway act as upstream signals that activate the NFκB signaling pathway. Upon activation, the NFκB pathway promotes the transcription and expression of related inflammatory factors, including key targets predicted by PPI such as IL-6, TNF-α and COX-2. TNF-α can activate the TNF signaling pathway, COX-2 can activate Arachidonic acid metabolism, and IL-6 can activate the JAK/STAT signaling pathway.

Previous studies have shown that these inflammatory factors are highly expressed in the liver during methotrexate-induced liver injury and contribute to hepatocyte apoptosis.⁵⁷ Furthermore, several studies have suggested that TGP exerts inhibitory effects on the PI3K/AKT, MAPK, and NFκB pathways, and can suppress the production of related inflammatory factors.⁵⁸ Therefore, we hypothesize that TGP alleviates methotrexate-induced liver injury and inhibits the inflammatory response, likely through the inhibition of these pathways, thereby reducing hepatocyte necrosis by mitigating a series of inflammatory reactions and exerting a hepatoprotective effect.

Experimental results showed that in the methotrexate-induced liver injury mouse model, the expression of IL-6, TNF-α and COX-2 mRNA and protein in the liver was significantly elevated, while TGP effectively inhibited the expression of IL-6, TNF-α and COX-2 mRNA and protein. Additionally, the liver tissues of the methotrexate-induced injury mouse model showed significantly increased expression of p-AKT, p38-MAPK, and p-NFκB p65, suggesting that the PI3K signaling pathway, MAPK signaling pathway, and NFκB signaling pathway were abnormally activated, which can be reversed by TGP intervention.

Conclusion and Limitation

The present study demonstrates that TGP effectively alleviates MILI by reducing serum ALT and AST levels, improving liver histopathology, and suppressing inflammatory responses through modulation of PI3K/AKT, NFκB, and MAPK signaling pathways. Network pharmacology and metabolomics revealed that TGP's hepatoprotective effects are mediated via key targets and pathways, including arachidonic acid metabolism and steroid hormone biosynthesis, which synergistically mitigate hepatocyte apoptosis and inflammatory cascades. However, this study has limitations. First, the mechanism validation focused primarily on mRNA and protein expression levels, lacking direct functional assays to confirm pathway interactions. Second, the translational relevance of findings from a murine model to human clinical scenarios requires further investigation, particularly regarding TGP's pharmacokinetics and long-term safety. Additionally, the untargeted metabolomics approach, while comprehensive, may overlook low-abundance metabolites critical to MILI pathogenesis. Future studies should integrate multi-omics analyses and clinical trials to validate TGP's therapeutic potential and optimize its application in mitigating drug-induced hepatotoxicity.

Funding

This study was supported by the National Natural Science Foundation of China (No. 81673941).

Disclosure

The authors report no conflicts of interest in this work.

References

- Björnsson HK, Björnsson ES. Drug-induced liver injury: pathogenesis, epidemiology, clinical features, and practical management. *Eur J Intern Med.* 2022;97:26–31. doi:10.1016/j.ejim.2021.10.035
- Liang D, Guan Y, Zhu J, et al. Global research trends of drug-induced liver injury (DILI) in the past two decades: a bibliometric and visualized study. *Ann Palliat Med.* 2021;10(8):8651–8664. doi:10.21037/apm-21-981
- Jaeschke H, Akakpo JY, Umbaugh DS, Ramachandran A. Novel therapeutic approaches against acetaminophen-induced liver injury and acute liver failure. *Toxicol Sci.* 2020;174(2):159–167. doi:10.1093/toxsci/kfaa002
- Li ZB, Chen DD, He QJ, et al. The LAC score indicates significant fibrosis in patients with chronic drug-induced liver injury: a large biopsy-based study. *Front Pharmacol.* 2021;12:734090. doi:10.3389/fphar.2021.734090
- Chrysostomou D, Roberts LA, Marchesi JR, Kinross JM. Gut microbiota modulation of efficacy and toxicity of cancer chemotherapy and immunotherapy. *Gastroenterology.* 2023;164(2):198–213. doi:10.1053/j.gastro.2022.10.018
- AlAmeel T, Al Sulais E, Raine T. Methotrexate in inflammatory bowel disease: a primer for gastroenterologists. *Saudi J Gastroenterol.* 2022;28(4):250–260. doi:10.4103/sjg.sjg_496_21
- Zhao Z, Hua Z, Luo X, et al. Application and pharmacological mechanism of methotrexate in rheumatoid arthritis. *Biomed Pharmacother.* 2022;150:113074. doi:10.1016/j.biopha.2022.113074
- Hamed KM, Dighriri IM, Baomar AF, et al. Overview of methotrexate toxicity: a comprehensive literature review. *Cureus.* 2022;14(9):e29518. doi:10.7759/cureus.29518
- Hu Q, Wang H, Xu T. Predicting hepatotoxicity associated with low-dose methotrexate using machine learning. *J Clin Med.* 2023;12(4):1599. doi:10.3390/jcm12041599
- Di Martino V, Verhoeven DW, Verhoeven F, et al. Busting the myth of methotrexate chronic hepatotoxicity. *Nat Rev Rheumatol.* 2023;19(2):96–110. doi:10.1038/s41584-022-00883-4
- Anonymous. *Shennong Bencao Jing*. Beijing: China Medical Science Press; 2018.
- Jiang H, Li J, Wang L, et al. Total glucosides of paeony: a review of its phytochemistry, role in autoimmune diseases, and mechanisms of action. *J Ethnopharmacol.* 2020;258:112913. doi:10.1016/j.jep.2020.112913
- Xu R, Peng J, Ma Z, et al. Prolonged administration of total glucosides of paeony improves intestinal immune imbalance and epithelial barrier damage in collagen-induced arthritis rats based on metabolomics-network pharmacology integrated analysis. *Front Pharmacol.* 2023;14:1187797. doi:10.3389/fphar.2023.1187797
- Liang CL, Jiang H, Feng W, et al. Total glucosides of paeony ameliorate pristane-induced lupus nephritis by inducing PD-1 ligands(+) macrophages via activating IL-4/STAT6/PD-L2 signaling. *Front Immunol.* 2021;12:683249. doi:10.3389/fimmu.2021.683249
- Su L, Lu H, Zhang D, et al. Total paeony glycoside relieves neuroinflammation to exert antidepressant effect via the interplay between NLRP3 inflammasome, pyroptosis and autophagy. *Phytomedicine.* 2024;128:155519. doi:10.1016/j.phymed.2024.155519
- Xiu Y, Wang S, Zhang P, et al. Total glucosides of paeony alleviates cGAS-STING-mediated diseases by blocking the STING-IRF3 interaction. *Chin J Nat Med.* 2024;22(5):402–415. doi:10.1016/S1875-5364(24)60572-8
- Zhao M, Peng N, Zhou Y, et al. The immunoregulatory effects of total glucosides of paeony in autoimmune diseases. *J Leukoc Biol.* 2024;16:qiae095.
- Su T, Jiang WY, Gao L. Study on industrial extraction process of total glucosides of paeoniae albiflora. *Electron J Clin Med Lit.* 2015;2(11):2015–2017.
- Li S, Wang YN, Liu XY, et al. Research on extraction and purification processes of total glucosides of paeoniae albiflora. *Food Sci.* 2007; (5):173–176.
- Luo J, Jin DE, Yang GY, et al. Total glucosides of paeony for rheumatoid arthritis: a systematic review of randomized controlled trials. *Complement Ther Med.* 2017;34:46–56. doi:10.1016/j.ctim.2017.07.010
- Zhu X, Shen X, Hou X, et al. Total glucosides of paeony for the treatment of rheumatoid arthritis: a methodological and reporting quality evaluation of systematic reviews and meta-analyses. *Int Immunopharmacol.* 2020;88:106920. doi:10.1016/j.intimp.2020.106920
- Yang K, Zeng L, Long Z, et al. Efficacy and safety of total glucosides of paeony in the treatment of 5 types of inflammatory arthritis: a systematic review and meta-analysis. *Pharmacol Res.* 2023;195:106842. doi:10.1016/j.phrs.2023.106842
- Zhang Y, Wang X, Ding Z, Lin N, Zhang Y. Enhanced efficacy with reduced toxicity of tripterygium glycoside tablet by compatibility with total glucosides of paeony for rheumatoid arthritis therapy. *Biomed Pharmacother.* 2023;166:115417. doi:10.1016/j.biopha.2023.115417
- Huang Y, Wang H, Chen Z, et al. Efficacy and safety of total glucosides of paeony combined with methotrexate and leflunomide for active rheumatoid arthritis: a meta-analysis. *Drug Des Devel Ther.* 2019;13:1969–1984. doi:10.2147/DDDT.S207226
- Xiang N, Li XM, Zhang MJ, et al. Total glucosides of paeony can reduce the hepatotoxicity caused by methotrexate and leflunomide combination treatment of active rheumatoid arthritis. *Int Immunopharmacol.* 2015;28(1):802–807. doi:10.1016/j.intimp.2015.08.008
- Zhang J, Fu Y, Yang B, Xiang X. Total glucosides of paeony inhibits liver fibrosis and inflammatory response associated with cirrhosis via the FLII/NLRP3 axis. *Am J Transl Res.* 2022;14(6):4321–4336.
- Elsawy H, Algefare AI, Alfwuaires M, et al. Naringin alleviates methotrexate-induced liver injury in male albino rats and enhances its antitumor efficacy in HepG2 cells. *Biosci Rep.* 2020;40(6):BSR20193686. doi:10.1042/BSR20193686
- Schmidt S, Messner CJ, Gaiser C, Hämmerli C, Suter-Dick L. Methotrexate-induced liver injury is associated with oxidative stress, impaired mitochondrial respiration, and endoplasmic reticulum stress in vitro. *Int J Mol Sci.* 2022;23(23):15116. doi:10.3390/ijms232315116
- Al Kury LT, Dayyan F, Ali Shah F, et al. Ginkgo biloba extract protects against methotrexate-induced hepatotoxicity: a computational and pharmacological approach. *Molecules.* 2020;25(11):2540. doi:10.3390/molecules25112540
- Sahindokuyucu-Kocasarı F, Akyol Y, Özmen O, Erdemli-Köse SB, Garlı S. Apigenin alleviates methotrexate-induced liver and kidney injury in mice. *Hum Exp Toxicol.* 2021;40(10):1721–1731. doi:10.1177/09603271211009964
- Zhang B, Jiang G, Wang L, et al. An analysis of silybin meglumine tablets in the treatment of drug-induced liver injury as assessed for causality with the updated rousssel uclaf causality assessment method using a nationwide database. *Br J Clin Pharmacol.* 2023;89(4):1329–1337. doi:10.1111/bcp.15575
- Xu ZK, Wang QL, Wang C, Wei W. Protective effect of CP-25 on methotrexate-induced liver injury in rats and its molecular mechanism. *J Anhui Med Univ.* 2023;58(4):676–682.

33. Ru J, Li P, Wang J, et al. TCMSp: a database of systems pharmacology for drug discovery from herbal medicines. *J Cheminform.* 2014;6(1):13. doi:10.1186/1758-2946-6-13
34. Chen GY, Liu XY, Chen JQ, et al. Prediction of rhizoma drynariae targets in the treatment of osteoarthritis based on network pharmacology and experimental verification. *Evid Based Compl Alternat Med.* 2021;2021:5233462. doi:10.1155/2021/5233462
35. Jin Q, Li J, Chen GY, et al. Network and experimental pharmacology to decode the action of wendan decoction against generalized anxiety disorder. *Drug Des Devel Ther.* 2022;16:3297–3314. doi:10.2147/DDDT.S367871
36. Chen GY, Luo J, Luo Y, Yu XB, Liu XY, Tao QW. Network pharmacology analysis and experimental validation to investigate the mechanism of total flavonoids of rhizoma drynariae in treating rheumatoid arthritis. *Drug Des Devel Ther.* 2022;16:1743–1766. doi:10.2147/DDDT.S354946
37. Chen GY, Liu XY, Luo J, Yu XB, Liu Y, Tao QW. Integrating network pharmacology and experimental validation to explore the key mechanism of gubitong recipe in the treatment of osteoarthritis. *Comput Math Methods Med.* 2022;2022:7858925. doi:10.1155/2022/7858925
38. Chen GY, Wang YF, Yu XB, et al. Network pharmacology-based strategy to investigate the mechanisms of cibotium barometz in treating osteoarthritis. *Evid Based Complement Alternat Med.* 2022;2022(1):1826299.
39. Chen GY, Liu XY, Yan XE, et al. total flavonoids of rhizoma drynariae treat osteoarthritis by inhibiting arachidonic acid metabolites through AMPK/NFκB pathway. *J Inflamm Res.* 2023;16:4123–4140. doi:10.2147/JIR.S418345
40. Pundir S, Martin MJ, O'Donovan C. UniProt Consortium UniProt Tools. *Curr Protoc Bioinformatics.* 2016;53(1):1.29.1–1.29.15. doi:10.1002/0471250953.bi0129s53
41. Stelzer G, Rosen N, Plaschkes I, et al. The geneCards suite: from gene data mining to disease genome sequence analyses. *Curr Protoc Bioinformatics.* 2016;54(1):1.30.1–1.30.33. doi:10.1002/cpbi.5
42. Szklarczyk D, Kirsch R, Koutrouli M, et al. The STRING database in 2023: protein-protein association networks and functional enrichment analyses for any sequenced genome of interest. *Nucleic Acids Res.* 2023;51(D1):D638–D646. doi:10.1093/nar/gkac1000
43. Zhou Y, Zhou B, Pache L, et al. Metascape provides a biologist-oriented resource for the analysis of systems-level datasets. *Nat Commun.* 2019;10(1):1523. doi:10.1038/s41467-019-09234-6
44. Hu Z, Escalera-Joy AM, Ashcraft E, et al. Clinical risk factors for high-dose methotrexate-induced oral mucositis following individualized dosing. *Cancer Med.* 2024;13(21):e70351. doi:10.1002/cam4.70351
45. Koźmiński P, Halik PK, Chesori R, Gniazdowska E. Overview of dual-acting drug methotrexate in different neurological diseases, autoimmune pathologies and cancers. *Int J Mol Sci.* 2020;21(10):3483. doi:10.3390/ijms21103483
46. Rababa'h AM, Hussein SA, Khabour OF, Alzoubi KH. The protective effect of cilostazol in genotoxicity induced by methotrexate in human cultured lymphocytes. *Curr Mol Pharmacol.* 2020;13(2):137–143. doi:10.2174/1874467212666191023120118
47. Cronstein BN, Aune TM. Methotrexate and its mechanisms of action in inflammatory arthritis. *Nat Rev Rheumatol.* 2020;16(3):145–154. doi:10.1038/s41584-020-0373-9
48. Sandhu A, Ahmad S, Kaur P, Bhatnagar A, Dhawan V, Dhir V. Methotrexate preferentially affects Tc1 and Tc17 subset of CD8 T lymphocytes. *Clin Rheumatol.* 2019;38(1):37–44. doi:10.1007/s10067-018-4011-8
49. Shetty A, Cho W, Alazawi W, Syn WK. Methotrexate hepatotoxicity and the impact of nonalcoholic fatty liver disease. *Am J Med Sci.* 2017;354(2):172–181. doi:10.1016/j.amjms.2017.03.014
50. Wilsmann-Theis D, Funk R, Mössner R, Bieber T, Wenzel J. Efficacy and safety of methotrexate in psoriasis vulgaris long-term treatment: a real-world observation study. *Indian J Dermatol.* 2023;68(6):669–673. doi:10.4103/ijd.ijd_551_23
51. Taru V, Szabo G, Mehal W, Reiberger T. Inflammasomes in chronic liver disease: hepatic injury, fibrosis progression and systemic inflammation. *J Hepatol.* 2024;81(5):895–910. doi:10.1016/j.jhep.2024.06.016
52. Qian Y, Zhao J, Wu H, Kong X. Innate immune regulation in inflammation resolution and liver regeneration in drug-induced liver injury. *Arch Toxicol.* 2025;99(1):115–126. doi:10.1007/s00204-024-03886-0
53. Wang Y, Zhang H, Du G, et al. Total glucosides of paeony (TGP) inhibits the production of inflammatory cytokines in oral lichen planus by suppressing the NF-κB signaling pathway. *Int Immunopharmacol.* 2016;36:67–72. doi:10.1016/j.intimp.2016.04.010
54. Xu XX, Qi XM, Zhang W, et al. Effects of total glucosides of paeony on immune regulatory toll-like receptors TLR2 and 4 in the kidney from diabetic rats. *Phytomedicine.* 2014;21(6):815–823. doi:10.1016/j.phymed.2013.12.003
55. Jin Y, Zhang A. Total glucosides of paeony ameliorates oxidative stress, apoptosis and inflammatory response by regulating the smad7-TGF-β pathway in allergic rhinitis. *Mol Med Rep.* 2022;25(3):83. doi:10.3892/mmr.2022.12599
56. Jiang T, Guo J, Wang Y, et al. Total glucosides of paeony alleviates experimental Sjögren's syndrome through inhibiting NLRP3 inflammasome activation of submandibular gland cells. *Clin Exp Rheumatol.* 2023;41(12):2502–2510. PMID: 38149512. doi:10.55563/clinexprheumatol/7kbuok
57. Zhang L, Wei W. Anti-inflammatory and immunoregulatory effects of paeoniflorin and total glucosides of paeony. *Pharmacol Ther.* 2020;207:107452. doi:10.1016/j.pharmthera.2019.107452
58. Zhang S, Zhang J, Zhang X, Lv P, Guo S. The protective effect of total glucosides of white paeony capsules on experimental autoimmune encephalomyelitis. *Immunobiology.* 2023;228(2):152313. doi:10.1016/j.imbio.2022.152313

Drug Design, Development and Therapy

Publish your work in this journal

Drug Design, Development and Therapy is an international, peer-reviewed open-access journal that spans the spectrum of drug design and development through to clinical applications. Clinical outcomes, patient safety, and programs for the development and effective, safe, and sustained use of medicines are a feature of the journal, which has also been accepted for indexing on PubMed Central. The manuscript management system is completely online and includes a very quick and fair peer-review system, which is all easy to use. Visit <http://www.dovepress.com/testimonials.php> to read real quotes from published authors.

Submit your manuscript here: <https://www.dovepress.com/drug-design-development-and-therapy-journal>

Dovepress
Taylor & Francis Group